Front. Phys. 12(3), 127203 (2017)
DOI 10.1007/s11467-016-0629-7

RESEARCH ARTICLE

Carrier balance and linear magnetoresistance in type-II Weyl semimetal WTe_2

Xing-Chen Pan[1], Yiming Pan[1], Juan Jiang[2], Huakun Zuo[3], Huimei Liu[1], Xuliang Chen[4], Zhongxia Wei[1], Shuai Zhang[1], Zhihe Wang[1], Xiangang Wan[1], Zhaorong Yang[4], Donglai Feng[2], Zhengcai Xia[3], Liang Li[3], Fengqi Song[1,*], Baigeng Wang[1,†], Yuheng Zhang[4], Guanghou Wang[1]

[1] *National Laboratory of Solid State Microstructures, Collaborative Innovation Center of Advanced Microstructures, and College of Physics, Nanjing University, Nanjing 210093, China*
[2] *State Key Laboratory of Surface Physics, Collaborative Innovation Center of Advanced Microstructures, Department of Physics, and Advanced Materials Laboratory, Fudan University, Shanghai 200433, China*
[3] *Wuhan National High Magnetic Field Center, Huazhong University of Science and Technology, Wuhan 430074, China*
[4] *High Magnetic Field Laboratory, Chinese Academy of Sciences, Hefei 230031, China*
*Corresponding authors. E-mail: *songfengqi@nju.edu.cn, †bgwang@nju.edu.cn*

Received September 3, 2016; accepted October 8, 2016

Unsaturated magnetoresistance (MR) has been reported in type-II Weyl semimetal WTe_2, manifested as a perfect compensation of opposite carriers. We report linear MR (LMR) in WTe_2 crystals, the onset of which was identified by constructing the MR mobility spectra for weak fields. The LMR further increased and became dominant for fields stronger than 20 T, while the parabolic MR gradually decayed. The LMR was also observed in high-pressure conditions.

Keywords WTe_2, type-II Weyl semimetal, carrier balance, linear magnetoresistance

PACS numbers 75.47.Np, 72.15.-v, 71.20.G

1 Introduction

The type-II Weyl semimetal phase, a novel state of topological quantum matter, with its band structure containing strongly tilted Weyl cones, has attracted significant attention owing to its unique electronic structure and transport properties [1–6]. Different from type-I Weyl semimetals, which possess a point-like Fermi surface at the Weyl point, the Weyl points of a typical type-II Weyl semimetal exist at the boundaries between electron and hole pockets [1–5]. On the surface of a Weyl semimetal, spin-polarized topological Fermi arcs connect the projections of Weyl points with opposite chirality [6]. Type-II Weyl semimetals can constitute a novel platform for exploring exotic quantum phenomena.

WTe_2 was predicted to be a type-II Weyl semimetal [1]. Novel physical properties of this material have recently been discovered, related to its extremely high (on the order of 10^6) magnetoresistance (MR), which remains unsaturated in fields as strong as 60 T [7]. Angle-resolved photoemission spectroscopy (ARPES) revealed that equal-sized electron/hole pockets at low-temperature Fermi levels [8] also manifested as quantum oscillations [9, 10]. In addition, this crystal exhibited superconducting properties under an applied pressure of 2.5 GPa [10, 11], reproducing the dome-like pressure-superconductivity temperature phase diagram of MoS_2 [12]. One-dimensional transport through its atomic chains has been suggested, based on longitudinal MR measurements in optimal configurations [11]. Most recently, an ARPES study using polarized light demonstrated a circular dichroism, indicating novel physical phenomena related to exotic spin textures [13].

Here, we show that this crystal exhibits linear MR (LMR). The LMR was visualized using weak-field MR mobility spectra, and remained unsaturated in fields as strong as 60 T. This observation lends a strong support to the MR non-saturation and universality. Our work implies that WTe_2 is a multifunctional candidate for advanced 2D materials.

---

*Special Topic: Recent Progress on Weyl Semimetals (Eds. Xincheng Xie, Xian-Gang Wan, Hong-Ming Weng & Hua Jiang).
arXiv: 1505.07968.

2 Experimental results

WTe_2 single crystals were grown using the $TeBr_4$ transport method and characterized by X-ray diffraction, as described elsewhere [10]. The measurements of transport under pressure were performed using a custom system designed in the Hefei High Magnetic Field Laboratory. Its diamond anvil cell has been described elsewhere [10]. Daphne 7373 oil was employed as the pressure-transmitting medium. The ambient-pressure electrical transport measurements were performed in a Cryomagnetics cryostat in Nanjing University. Ohmic contacts were made using gold wires and a silver paste. High-resolution ARPES was used for obtaining the electronic structure. ARPES experiments were performed at the I05 beamline of Diamond Light Source (DLS) equipped with a Scienta R4000 electron analyzer. The angular resolution was 0.3° and the overall energy resolution was higher than 10 meV. The samples were cleaved in situ along the (001) plane and measured in ultra-high vacuum (below 5×10^{-10} Torr). The results obtained are shown in Fig. 1. A series of Fermi pockets was observed after mapping the Fermi surface, as summarized in Fig. 1(a). For each of the cuts in Fig. 1(a), the corresponding photoemission intensity mappings are shown in Figs. 1(b)–(e). The corresponding momentum distribution curves (MDCs) are shown in Figs. 1(f)–(i). By connecting the MDC peaks with dashed lines, several quasi-straight lines were obtained. In addition, all of the bands had rather high Fermi velocities, ranging from 1.7×10^5 to 2.1×10^5 m/s. Such electronic structures can be compared with ambient-pressure calculations.

An elaborate transport description of a single crystal of WTe_2 can be obtained using the mobility spectrum method, which extracts the carrier density, mobility, and strength of all the effective transport components. Such spectra have been useful for successfully obtaining transport descriptions of a number of multi-band systems, e.g., a two-dimensional electron gas [14], doped semiconductors [15], semi-metals [16] and iron-based superconductors [17, 18]. Here, we used this method to demonstrate the LMR signature, as well as the (expected) balance of electron- and hole-like carriers at low temperatures.

In general, for a sample involving more than one channel/type of carriers, the conductivity tensor components can be described as a sum over the m pockets (species) present within the multi-carrier fitting (MCF) system. In this procedure, the carrier densities n_m and the corresponding mobilities μ_m are the fitting parameters, where the number and type of carriers need to be assumed (typically between 2 and 5). The main drawback of the MCF procedure is its arbitrariness. A major advantage of the mobility spectrum analysis (MSA) over the MCF procedure is that the former is inherently non-arbitrary, i.e., no prior assumptions regarding the number or type of carriers are required. The resulting mobility spectra [19, 20] are more useful for analyzing the electrical conduction and carrier properties, compared with conventionally obtained concentrations and mobilities.

The conductivity tensor obtained from magnetoresistance and Hall effect data can be transformed into carrier density as a function of mobility; the result is known

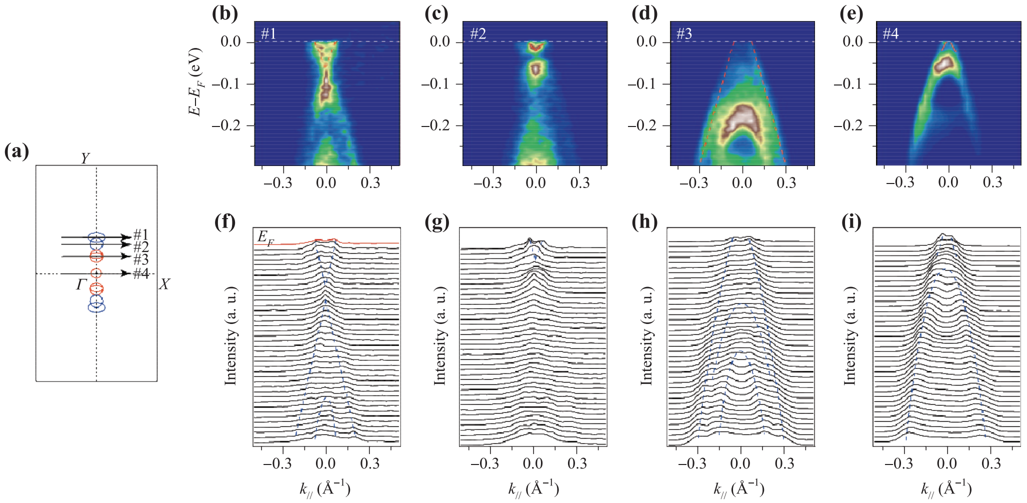

Fig. 1 Electronic structure of WTe_2 along the Γ-X direction from ARPES measurements. **(a)** Schematic of the Fermi surface of WTe_2. The red circles refer to the hole pockets, while the blue ones refer to the electron pockets. Different cuts are indicated by the black arrows. **(b–e)** Photoemission intensity plot along cut 1, cut 2, cut 3, and cut 4, respectively. The hole bands and electron bands are indicated by the red lines as a guide. **(f–i)** The corresponding momentum distribution curves of the spectra shown in panel (b–e), respectively. The blue dashed lines are traced from the MDC peaks to shown the dispersion of the bands.

as the mobility spectrum. Rather than making assumptions about the number of electron and hole pockets, the starting point of the MSA method is to allow the existence within the sample of a continuous distribution of electron-like and hole-like carriers of any mobility. Therefore, the reduced conductivity tensor is

$$\sigma_{xx} = \sigma^n_{xx} + \sigma^p_{xx} = \int \frac{s^{(n)}(\mu)}{1+\mu^2B^2}\mathrm{d}\mu + \int \frac{s^{(p)}(\mu)}{1+\mu^2B^2}\mathrm{d}\mu,$$

$$\sigma_{xy} = \sigma^n_{xy} + \sigma^p_{xy} = -\int \frac{s^{(n)}(\mu)\mu B}{1+\mu^2B^2}\mathrm{d}\mu + \int \frac{s^{(p)}(\mu)\mu B}{1+\mu^2B^2}\mathrm{d}\mu,$$

where the reduced conductivities are normalized to the conductivity σ_0 in the absence of a magnetic field. In the above equation, σ^n and σ^p denote partial longitudinal and transverse conductivities owing to electron-like or hole-like carriers. Instead of assuming the number of electron and hole pockets, we define the two continuously distributions of normalized conductivity versus mobility $s^{(n)}(\mu)$ and $s^{(p)}(\mu)$. Electron and hole pockets then appear as mobility peaks in the mobility spectrum. If the electron and hole terms could be separated, the number and the average mobility of different carrier types could be given as

$$K = \frac{\sigma_0}{e}\int \frac{s^{(k)}(\mu)}{\mu}\mathrm{d}\mu,$$

$$\bar{\mu} = \frac{\sigma_0 \int s^{(k)}(\mu)\mathrm{d}\mu}{eK}.$$

The parameters K (i.e., n, p) and $\bar{\mu}$ are calculated for a selected range of temperatures. The separation of the two types of partial conductivities can be obtained using the Kramers–Kronig (KK) relations, yielding

$$\frac{P}{\pi}\int \frac{\sigma_{xx}}{B-B'}\mathrm{d}B' = -\sigma^n_{xy} + \sigma^p_{xy},$$

$$\frac{P}{\pi}\int \frac{\sigma_{xy}}{B-B'}\mathrm{d}B' = \sigma^n_{xx} - \sigma^p_{xx}.$$

Here, P denotes the principal part of the integral and the integration limits are from negative infinity to positive infinity. Practically, for analytical calculations of the KK transformation, conductivity data are fitted to linear combinations of Lorentzian components within the MCF. In our case, a linear combination of three Lorentzian components was used to represent σ_{xx}, whereas up to five components were necessary to reproduce σ_{xy}. However, it should be noted that the MCF parameters are just an analytical presentation of the experimental data. A detailed description of the algorithm used in numerical calculations can be found in the literature cited in Refs. [19, 20]. To estimate the mobility spectra and avoid the inherent instability in the final spectrum, we discretized the mobility space as a logarithmic equally spaced grid, including up to 500 points. The continuous spectra obtained from the σ_{xx} datasets are shown in Fig. 3, and the results agree well with those independently obtained from σ_{xy}.

For analytical calculations of the KK transformation, we attempted to find a representation of the raw data. Therefore, we fitted the real G_{xx} and G_{xy} data to linear combinations of Lorentzian components

$$G_{xx}(B) = \sum_i \frac{\alpha_i}{1+\mu^2_{\alpha,i}B^2},$$

$$G_{xy}(B) = \sum_i \frac{\beta_i B}{1+\mu^2_{\beta,i}B^2}.$$

Note that the parameters α_i, β_i, and μ_i provide an analytical representation of the experimental data but have no physical meaning, compared with multi-band modeling. Here, we used a linear combination of three Lorentzian components to represent $G_{xx}(B)$, and a linear combination of five Lorentzian components to represent $G_{xy}(B)$.

We collected magneto-transport data for $\mathrm{WTe_2}$ single crystals at various temperatures. The crystalline structure of $\mathrm{WTe_2}$ is shown in Fig. 2(a). The inset of Fig. 2(b) shows a high-resolution transmission electron microscopy image of a typical single crystal and its Fourier transformation. A photograph of a typical sample is shown in the upper panel of Fig. 2(c), where its smooth, shiny appearance confirms its crystalline nature. A magnetic field (H) was applied parallel to the c-axis and a current was passed along the a-axis (W chains), respectively. The MR was defined by $[\rho_{xx}(H) - \rho(0)]/\rho(0)$. The MR and Hall resistivity for temperatures in the 1.7–77 K range are shown for a typical sample in Fig. 2(c). For $\mathrm{WTe_2}$, the MR increases in an almost parabolic manner (according to H^2), reproducing previously reported results [7, 11, 19]. Quantum oscillations were observed in the presence of a magnetic field of a few Tesla, as shown in Fig. 2(c), indicating high-quality crystals. The Hall resistivity was strongly nonlinearly dependent on the magnetic field intensity, suggesting a multi-band picture of transport in $\mathrm{WTe_2}$. Interestingly, a "turn on" effect in the longitudinal resistivity ρ_{xx} [7] may be observed in the temperature dependence of the Hall coefficient [defined as $\rho_{yx}/(\mu_0 H)$] for various magnetic fields.

The mobility spectra were constructed according to the MR data, as shown in Fig. 3. We first obtained the normalized conductivity matrix $\sigma_{ij}(H)/\sigma(0)$ from the resistivity matrix $\rho_{ij}(H)$ at 4.2 K, as shown in Fig. 3(a). To obtain an analytical representation of the transport data, we fitted a normalized conductivity matrix using a linear combination of Lorentzian components. The KK transformations were then performed on the analytical representations, for separating the contributions made by electron- and hole-like carriers. The partial conductivities of all of the electron- and hole-like components

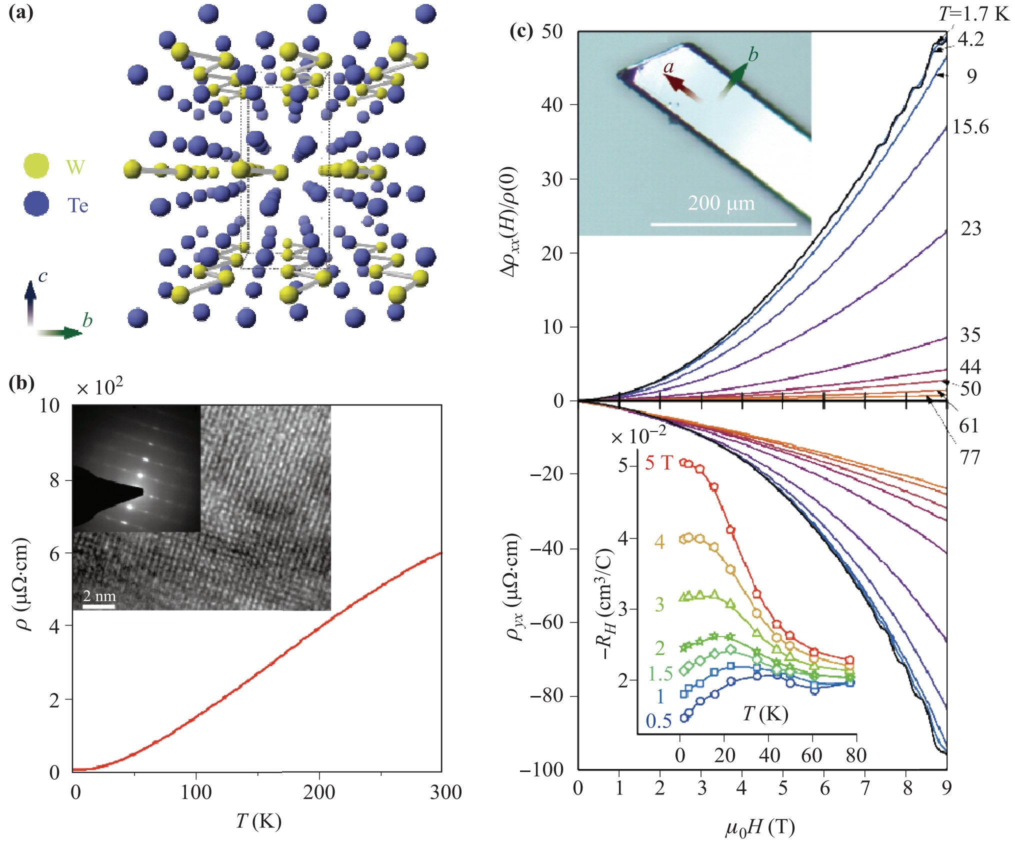

Fig. 2 Transport measurements for a WTe_2 single crystal. **(a)** Schematic crystal structure of WTe_2. **(b)** Temperature dependence of electrical resistivity. Inset: High-resolution TEM image of the crystal and its Fourier transformation (inset). **(c)** Upper panel: The magnetoresistance with $H//c$ up to 9 T at temperatures as shown. Inset: Photograph of a single crystal. Lower panel: The field-dependent Hall resistivity ρ_{yx}. Inset: Hall coefficient versus temperature at magnetic fields as shown.

obtained from the KK transformations are shown as the green and violet curves in Fig. 3(a), respectively. The contributions of the electron- and hole-like carriers can be deconvolved for temperatures in the 1.7–35 K range [20]. We finally obtained the mobility spectra at various temperatures by calculating the normalized conductivity matrix of the electron- and hole-like carriers as shown in Fig. 3(b). Although WTe_2 has a complicated Fermi surface with nine pockets [13], a single effective carrier component was clearly identified for the electron and hole sides at all temperatures considered.

The unsaturated MR in WTe_2 is believed to be a property of a compensated semi-metal, which occurs because the exactness of the compensation leads to a cancellation of the Hall-induced electrical field [7]. Our mobility spectra provide experimental evidence of the balance between the electron- and hole-like carriers in WTe_2. To obtain the carrier densities at various temperatures, we calculated the integrals of the mobility spectra for the data for temperatures in the 1.7–35 K range, and the results are shown in Fig. 3(c). The carriers' mobility at various temperatures can also be calculated from the positions of peaks in the mobility spectra [Fig. (3d)]. The mobility was nearly constant at temperatures under 10 K but gradually decreased as the temperature increased above 20 K. The carrier concentrations of the electron- (n) and hole- (p) like carriers were compared in the $(n-p)/(n+p)$ framework [Fig. 3(e)], and the two carrier types were found to be balanced, within an uncertainty of 2%. This supports theoretical predictions that an exact compensation ($n=p$) at low temperatures contributes to the non-saturating parabolic MR in this material, for magnetic fields reaching 60 T [7, 8, 21].

Interestingly, there is a long tail that shows an extreme mobility in the spectra at 4.2 K, while the spectra are rather more localized at 35 K, as shown in Fig. 3(b). We consider the long tail feature of the mobility spectra to be a signature of the LMR transport, i.e., $\sigma_{xx}^L \propto 1/B$. The LMR mobility spectra can be deduced from

$$\frac{1}{B} \propto \int \frac{s^L(\mu)}{1+\mu^2 B^2}\mathrm{d}\mu.$$

In the above equation, $s^L(\mu)$ is nearly constant, yield-

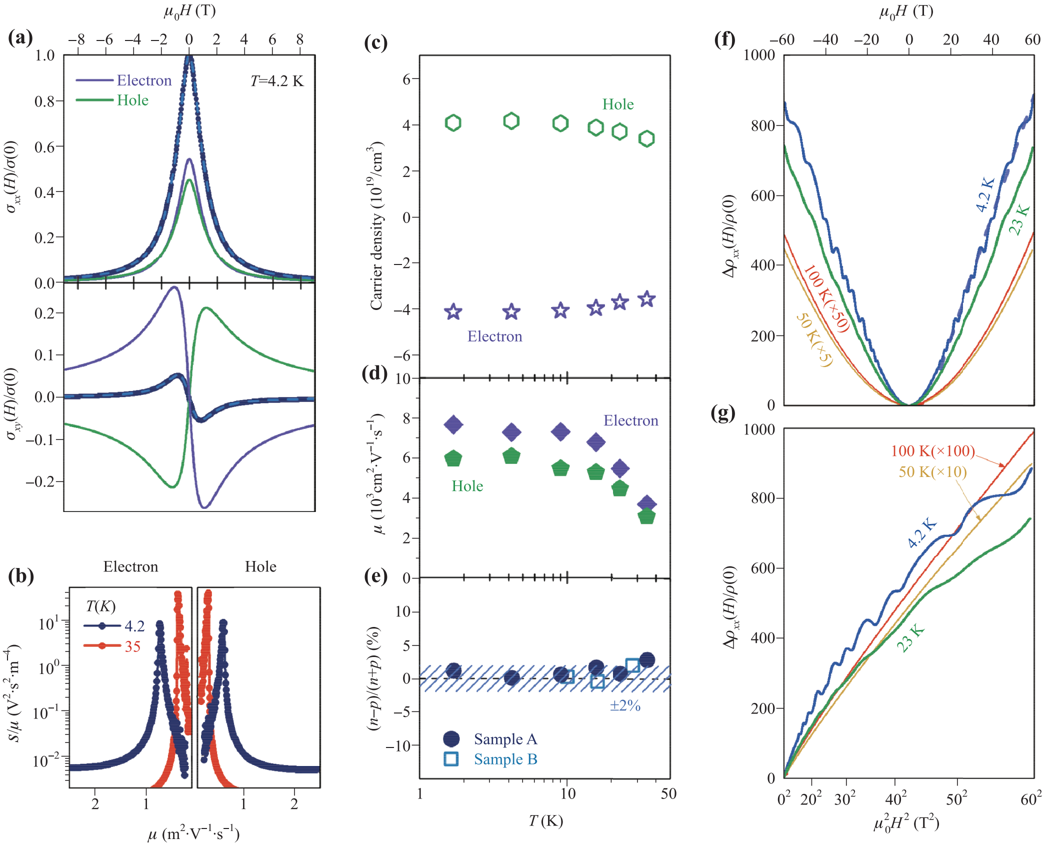

Fig. 3 Evidence of carrier balance and linear magnetoresistance (LMR) for a large field. **(a)** The normalized conductivities calculated from the experimental data at 4.2 K. The blue circles and dashed lines are the experimental data and their analytical representative curves, respectively. The solid lines show the partially normalized conductivities of electron-like (*violet*) and hole-like (*green*) carriers obtained from the Kronig–Kramer transformation. **(b)** Mobility (μ) spectra of electron-like (left) and hole-like (right) carriers at 4.2 (*blue*) and 35 K (*red*) showing the normalized carrier density per unit of μ against μ. Note the long tails up to the high mobility regions at 4.2 K. **(c)** Temperature dependence of the carrier density extracted from the mobility spectrum. **(d)** Temperature dependence of the carrier mobility. **(e)** The difference between the electron and hole populations in WTe_2, showing a perfect balance at low temperature. Sample A and B are from the same growth ampoule. **(f)** High-field MR measurements up to 60 T at different temperatures. At high field, the curves at low temperatures appear nearly H-linear. **(g)** Curves of MR versus H^2. The curves at high temperatures are almost linear in H^2.

ing a long tail that extends to the high-mobility spectral region $\frac{s^L(\mu)}{\mu}$, as shown in Fig. 3(b).

These long tails in the mobility spectra can be best understood in terms of the total conductivity tensor with a nontrivial component $\sim 1/H$, which does not exist in the semi-classical two-band isotropic model (with a parabolic dispersion). This has previously been related to the LMR in $BaFe_2As_2$ and FeSe [17, 18]. We therefore believe these results to be the signature of the LMR onset in the low-field transport in our material.

The LMR was observed and indeed predominated over the parabolic MR for magnetic fields stronger than 20 T, and remained unsaturated for fields reaching 60 T. As shown in Fig. 3(e), the MR data were measured at different temperatures for a pulsed high field. The MR increased monotonously as the field intensity increased up to an extreme value of 60 T, although some of the characteristics were attributed to Shubnikov–de Haas oscillations (SdHOs) at lower temperatures. Also note that the LMR was further developed at stronger fields as seen for the MR at 4.2 K, where the MR maintained its parabolic (semi-classical) behavior at weak fields and became entirely linear for fields above 20 T. This is clearly seen when inspecting the H^2 coordinate, as shown in Fig. 3(f). At the temperature of 100 K, the data are described by a linear relation [Fig. 3(f)], which implies a parabolic MR at the temperature of 100 K because the semi-classical component still dominates the total conductivity tensor at this temperature. The blue curve clearly deviates from the semi-classical MR in the strong-field regime at 4.2 K.

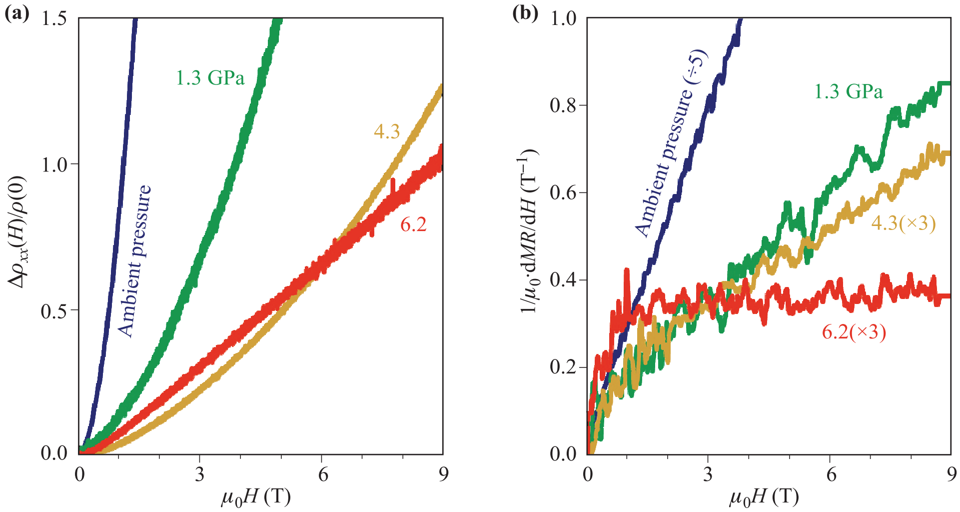

Fig. 4 Linear magnetoresistance under high-pressure. **(a)** Magnetoresistance at low temperature under ambient pressure, 1.3, 4.3, and 6.2 GPa. Linear MR was observed under 6.2 GPa. **(b)** The magnetic field derivatives of MR.

From the transport data, it is clear that the LMR trend tends to predominate at stronger fields and lower temperatures, indicating that it is an intrinsic property of WTe_2 crystals.

Our high-pressure experiments also revealed LMR. As shown in Fig. 4(a), our MR data were obtained at 1.3, 4.3, and 6.2 GPa, and the results were compared with the data obtained under ambient pressure. The high-pressure data were collected at 5 K, at which pressure-induced superconductivity does not occur [10]. The ambient-pressure experiment was conducted at 4.2 K. Firstly, MR was significantly suppressed (by more than one order of magnitude) under high pressure, consistent with previous reports [9–11]. SdHOs were not observed in high-pressure experiments, indicating the suppression of the carrier mobility. Secondly, a clear LMR was observed at a pressure of 6.2 GPa. The first derivatives of the MR with respect to the magnetic field are shown in Fig. 4(b). At ambient pressure, $\mathrm{d}MR/\mathrm{d}H$ was nearly linear in H, indicating an almost H^2 dependence of MR for the range of field intensities used. With increasing the pressure, $\mathrm{d}MR/\mathrm{d}H$ became nonlinear with respect to H. At 6.2 GPa, $\mathrm{d}MR/\mathrm{d}H$ became constant, and was independent of H. This indicates a perfect and robust LMR at high pressures, while the semi-classical parabolic MR, which underlies the significant MR non-saturation, fades out owing to the suppressed mobility or broken carrier balance.

3 Discussion

As previously discussed, no obvious structural transition was observed for pressures comparable to those used in our experiments. However, the density of states was very pressure-sensitive. The density of states increased rapidly as the pressure increased, suggesting that the carrier density might vary significantly [10]. Moreover, SdHOs at high pressures indicated that the Fermi surface was very pressure-sensitive. The results of both the calculations [10] and the experiments strongly suggest that the electron–hole balance may be broken at high pressures. This implies that LMR becomes dominant while the electron–hole balance is broken, as required for semi-classical MR unsaturation.

LMR has been reported in several metal/semi-metal single crystal materials, among which Cd_3As_2 [22, 23], TlBiSSe [24], and Na_3Bi [25] are Dirac semimetals and TaAs [26] and NbP [27] are Weyl semimetals. $BaFe_2As_2$ [28] exhibits some Dirac-cone-like structures. Quasi-linear band structures were observed in almost all of these materials with reported LMR, besides Bi_2Te_3 [29] and silver chalcogenides [30]. Linear magnetoresistance may be the fundamental property of topological metals [31]. Anisotropic linear magnetoresistance can also be observed when the magnetic field is parallel to the c-axis [32] which is different from this work.

4 Conclusion

In summary, carrier balance and LMR have been demonstrated in WTe_2 crystals. The LMR was observed at strong magnetic fields and low temperatures. When the parabolic semi-classical MR faded out owing to the broken carrier balance at high pressures, the LMR was also observed. This suggests potential applications of WTe_2 in spintronic devices.

Acknowledgements The authors would like to thank the National Key Projects for Basic Research in China (Grant Nos. 2013CB922103, 2015CB921202, and 2014CB921103), the National Natural Science Foundation of China (Grant Nos. 91421109, 11134005, 61176088, 51372112, 11522432, 11574288, and 2117109), the NSF of Jiangsu Province (Grant No. BK20130054), the PAPD project, and the Fundamental Research Funds for the Central Universities, for financially supporting this work. The technical assistance provided by Profs. Li Pi and Mingliang Tian of the Hefei High Field Center is also gratefully acknowledged. The insightful discussions with Prof. Haihu Wen from Nanjing University were also extremely helpful. We thank the help from Dr. P. Dudin, Dr. T. Kim, and Dr. M. Hoesch at DLS.

References and notes

1. A. A. Soluyanov, D. Gresch, Z. Wang, Q. S. Wu, M. Troyer, X. Dai, and B. A. Bernevig, Type-II Weyl semimetals, *Nature* 527(7579), 495 (2015)
2. S. Y. Xu, I. Belopolski, N. Alidoust, M. Neupane, G. Bian, C. Zhang, R. Sankar, G. Chang, Z. Yuan, C.C. Lee, S.M. Huang, H. Zheng, J. Ma, D. S. Sanchez, B. Wang, A. Bansil, F. Chou, P. P. Shibayev, H. Lin, S. Jia, and M. Z. Hasan, Discovery of a Weyl fermion semimetal and topological Fermi arcs, *Science* 349(6248), 613 (2015)
3. B. Q. Lv, H. M. Weng, B. B. Fu, X. P. Wang, H. Miao, J. Ma, P. Richard, X. C. Huang, L. X. Zhao, G. F. Chen, Z. Fang, X. Dai, T. Qian, and H. Ding, Experimental discovery of Weyl semimetal TaAs, *Phys. Rev. X* 5(3), 031013 (2015)
4. I. Belopolski, S.-Y. Xu, Y. Ishida, X.C. Pan, P. Yu, D. S. Sanchez, M. Neupane, N. Alidoust, G. Chang, T.-R. Chang, Y. Wu, G. Bian, H. Zheng, S.-M. Huang, C.-C. Lee, D. Mou, L. Huang, Y. Song, B. G. Wang, G. H. Wang, Y.-W. Yeh, N. Yao, J. Rault, P. Lefevre, F. Bertran, H.-T. Jeng, T. Kondo, A. Kaminski, H. Lin, Z. Liu, F. Q. Song, S. Shin, and M. Z. Hasan, Unoccupied electronic structure and signatures of topological Fermi arcs in the Weyl semimetal candidate $Mo_xW_{1-x}Te_2$, arXiv: 1512.09099 (2015)
5. I. Belopolski, S.Y. Xu, Y. Ishida, X. Pan, P. Yu, D. S. Sanchez, H. Zheng, M. Neupane, N. Alidoust, G. Chang, T.R. Chang, Y. Wu, G. Bian, S.M. Huang, C.C. Lee, D. Mou, L. Huang, Y. Song, B. Wang, G. Wang, Y.W. Yeh, N. Yao, J. E. Rault, P. Le Fèvre, F. Bertran, H.T. Jeng, T. Kondo, A. Kaminski, H. Lin, Z. Liu, F. Song, S. Shin, and M. Z. Hasan, Fermi arc electronic structure and Chern numbers in the type-II Weyl semimetal candidate $Mo_xW_{1-x}Te_2$, *Phys. Rev. B* 94(8), 085127 (2016)
6. X. G. Wan, A. M. Turner, A. Vishwanath, and S. Y. Savrasov, Topological semimetal and Fermi-arc surface states in the electronic structure of pyrochlore iridates, *Phys. Rev. B* 83(20), 205101 (2011)
7. M. N. Ali, J. Xiong, S. Flynn, J. Tao, Q. D. Gibson, L. M. Schoop, T. Liang, N. Haldolaarachchige, M. Hirschberger, N. P. Ong, and R. J. Cava, Large, non-saturating magnetoresistance in WTe_2, *Nature* 514, 205 (2014)
8. I. Pletikosić M. N. Ali, A. Fedorov, R. Cava, and T. Valla, Electronic structure basis for the extraordinary magnetoresistance in WTe_2, *Phys. Rev. Lett.* 113(21), 216601 (2014)
9. P. Cai, J. Hu, L. P. He, J. Pan, X. C. Hong, Z. Zhang, J. Zhang, J. Wei, Z. Q. Mao, and S. Y. Li, Drastic pressure effect on the extremely large magnetoresistance in WTe_2: Quantum oscillation study, *Phys. Rev. Lett.* 115(5), 057202 (2015)
10. X. C. Pan, X. Chen, H. Liu, Y. Feng, Z. Wei, Y. Zhou, Z. Chi, L. Pi, F. Yen, F. Song, X. Wan, Z. Yang, B. Wang, G. Wang, and Y. Zhang, Pressure-driven dome-shaped superconductivity and electronic structural evolution in tungsten ditelluride, *Nat. Commun.* 6, 7805 (2015)
11. D. Kang, Y. Zhou, W. Yi, C. Yang, J. Guo, Y. Shi, S. Zhang, Z. Wang, C. Zhang, S. Jiang, A. Li, K. Yang, Q. Wu, G. Zhang, L. Sun, and Z. Zhao, Superconductivity emerging from a suppressed large magnetoresistant state in tungsten ditelluride, *Nat. Commun.* 6, 7804 (2015)
12. J. Ye, Y. Zhang, R. Akashi, M. Bahramy, R. Arita, and Y. Iwasa, Superconducting dome in a gate-tuned band insulator, *Science* 338(6111), 1193 (2012)
13. J. Jiang, F. Tang, X. C. Pan, H. M. Liu, X. H. Niu, Y. X. Wang, D. F. Xu, H. F. Yang, B. P. Xie, F. Q. Song, P. Dudin, T. K. Kim, M. Hoesch, P. K. Das, I. Vobornik, X. G. Wan, and D. L. Feng, Signature of strong spin-orbital coupling in the large nonsaturating magnetoresistance material WTe_2, *Phys. Rev. Lett.* 115(16), 166601 (2015)
14. J. Antoszewski and L. Faraone, Quantitative mobility spectrum analysis (QMSA) in multi-layer semiconductor structures, *Opto-Electron. Rev.* 12, 347 (2004)
15. J. Antoszewski, G. Umana-Membreno, and L. Faraone, High-resolution mobility spectrum analysis of multicarrier transport in advanced infrared materials, *J. Electron. Mater.* 41(10), 2816 (2012)
16. J. McClure, Analysis of multicarrier galvanomagnetic data for graphite, *Phys. Rev.* 112(3), 715 (1958)
17. K. Huynh, Y. Tanabe, T. Urata, S. Heguri, K. Tanigaki, T. Kida, and M. Hagiwara, Mobility spectrum analytical approach for intrinsic band picture of $Ba(FeAs)_2$, *New J. Phys.* 16(9), 093062 (2014)
18. K. Huynh, Y. Tanabe, T. Urata, H. Oguro, S. Heguri, K. Watanabe, and K. Tanigaki, Electric transport of a single-crystal iron chalcogenide FeSe superconductor: Evidence of symmetry-breakdown nematicity and additional ultrafast Dirac cone-like carriers, *Phys. Rev. B* 90(14), 144516 (2014)

19. Z. Zhu, X. Lin, J. Liu, B. Fauque, Q. Tao, C. Yang, Y. Shi, and K. Behnia, Quantum oscillations, thermoelectric coefficients, and the Fermi surface of semimetallic WTe_2, *Phys. Rev. Lett.* 114(17), 176601 (2015)
20. At higher temperature, the mobility is strongly suppressed by electron-phonon interaction. The parameters obtained from the mobility spectra at higher temperatures are not exact.
21. H. Lv, W. Lu, D. Shao, Y. Liu, S. Tan, and Y. Sun, Perfect charge compensation in WTe_2 for the extraordinary magnetoresistance: From bulk to monolayer, *Europhys. Lett.* 110(3), 37004 (2015)
22. T. Liang, Q. Gibson, M. N. Ali, M. Liu, R. Cava, and N. Ong, Ultrahigh mobility and giant magnetoresistance in the Dirac semimetal Cd_3As_2, *Nat. Mater.* 14(3), 280 (2014)
23. A. Narayanan, M. D. Watson, S. F. Blake, N. Bruyant, L. Drigo, Y. L. Chen, D. Prabhakaran, B. Yan, C. Felser, T. Kong, P. C. Canfield, and A. I. Coldea, Linear magnetoresistance caused by mobility fluctuations in n-doped Cd_3As_2, *Phys. Rev. Lett.* 114(11), 117201 (2015)
24. M. Novak, S. Sasaki, K. Segawa, and Y. Ando, Large linear magnetoresistance in the Dirac semimetal TlBiSSe, *Phys. Rev. B* 91(4), 041203 (2015)
25. J. Xiong, S. Kushwaha, J. Krizan, T. Liang, R. Cava, and N. Ong, Anomalous conductivity tensor in the Dirac semimetal Na_3Bi, *EPL* 114(2), 27002 (2016)
26. C. Zhang, Z. Yuan, S. Xu, Z. Lin, B. Tong, M. Z. Hasan, J. Wang, C. Zhang, and S. Jia, Tantalum monoarsenide: An exotic compensated semimetal, arXiv: 1502.00251 (2015)
27. C. Shekhar, A. K. Nayak, Y. Sun, M. Schmidt, M. Nicklas, I. Leermakers, U. Zeitler, Y. Skourski, J. Wosnitza, Z. Liu, Y. Chen, W. Schnelle, H. Borrmann, Y. Grin, C. Felser, and B. Yan, Extremely large magnetoresistance and ultrahigh mobility in the topological Weyl semimetal candidate NbP, *Nat. Phys.* 11(8), 645 (2015)
28. K. K. Huynh, Y. Tanabe, and K. Tanigaki, Both electron and hole Dirac cone states in $Ba(FeAs)_2$ confirmed by magnetoresistance, *Phys. Rev. Lett.* 106(21), 217004 (2011)
29. D. X. Qu, Y. Hor, J. Xiong, R. Cava, and N. Ong, Quantum oscillations and Hall anomaly of surface states in the topological insulator Bi_2Te_3, *Science* 329(5993), 821 (2010)
30. R. Xu, A. Husmann, T. Rosenbaum, M. L. Saboungi, J. Enderby, and P. Littlewood, Large magnetoresistance in non-magnetic silver chalcogenides, *Nature* 390, 57 (1997)
31. J. C. W. Song, G. Refael, and P. A. Lee, Linear magnetoresistance in metals: Guiding center diffusion in a smooth random potential, *Phys. Rev. B* 92(18), 180204 (2015)
32. Y. Zhao, H. Liu, J. Yan, W. An, J. Liu, X. Zhang, H. Wang, Y. Liu, H. Jiang, Q. Li, Y. Wang, X.Z. Li, D. Mandrus, X. C. Xie, M. Pan, and J. Wang, Anisotropic magnetotransport and exotic longitudinal linear magnetoresistance in WTe_2 crystals, *Phys. Rev. B* 92(4), 041104(R) (2015)